Frequency-dependent circular-polarization of terahertz chiral spoof surface plasmon polariton on helically grooved metallic wire

Hai-Zi Yao[1], Shuncong Zhong[1,2] *

1 Laboratory of Optics, Terahertz and Non-destructive Testing, School of Mechanical Engineering and Automation, Fuzhou University, Fuzhou 350108, P. R. China

2 Department of Naval Architecture, Ocean and Marine Engineering, University of Strathclyde, Glasgow G4 0LZ, UK

* zhongshuncong@hotmail.com

Abstract: Chiral spoof surface plasmon polaritons in the terahertz region, resulting from a coherent superposition of TM and HE modes, can be generated by normally exciting helically corrugated metal wire with a linearly polarized Gaussian light. The handedness of the chiral SPP depends on the handedness of the helical groove. The chirality of the surface wave causes a spiral spatial extent of average power whose period is determined by the difference in the wave vector between two modes. Simultaneously, highly circular polarization of a confined surface wave emerges from the chirality of the geometry. Moreover, the polarization state is heavily dependent on working frequency relative to the characteristic frequency of each mode. This type of chiral SPP, originating from the helical groove, makes helically corrugated metal wire useful for some special applications, such as circularly polarized sources for terahertz near-field microscopy or terahertz sensors for chiral biomolecules.

Keywords: Terahertz, Chiral SPP, Circularly polarization

1. Introduction

As the underexplored gap of the electromagnetic field, terahertz (THz) has a unique advantage in many applications such as explosive detection [1-2], nondestructive evaluation for pharmaceutical tablets [3, 4] and spectroscopic analysis of proteins [5, 6] for many macromolecules that have vibrational frequencies in the THz frequency region [7-9]. A circularly polarized plane wave is chiral because it carries a nonzero angular momentum. Some important research in the fields of molecular spectroscopy and structural biology [10-12] are based on the interaction of chiral molecules and circularly polarized electromagnetic fields. Circularly polarized THz light is very important for studying macromolecular chiral structures, such as DNA or proteins. Especially for THz near-field microscopy, the sub-wavelength circularly polarized point source plays a great role. How to manipulate the polarization of radiation and shape EM fields at sub-wavelength scale dimensions has always been a hot issue [13, 14].

Surface plasmon polaritons (SPP), collective excitations of conduction electrons that only exist on the interface between metal and dielectric and enable electromagnetic waves to be localized and highly confined spatially, even to the nanometre dimension, play a potential role in addressing this challenge [15, 16]. Single metallic nanowire has attracted significant interest because it can be taken as an SPP waveguide, whose merit of nanometre-scale cross sections and capability of supporting SPP propagating a long distance relative to the incident wavelength make it broadly applicable in fields that require sub-wavelengths, such as dot source [17, 18] or single molecule sensor [19]. Recently, it was demonstrated theoretically and experimentally that the chiral SPP could be generated on metallic nanowire by properly controlling the incident polarization orientation [20-22], which may have a potential prospect as a sub-wavelength source of circular polarized photons.

However, the existence of a chiral mode on metal wire in the terahertz region has been rarely reported. This is mainly because compared with the intrinsic plasma frequency of noble metal, which generally lies in the visible and ultraviolet regions, terahertz is so low that metals responding to terahertz radiation resemble a perfectly electric conductor (PEC) that does not support SPP waves. Pendry et al. [23] outlined how the dispersion of surface EM modes could be engineered by texturing a surface. Even a perfectly electric conductor with a structured surface can sustain SPP-like modes (termed spoof SPP), resulting from a lowered effective plasma frequency determined completely by the surface geometry [24]. Therefore, surface structure facilitates an extension of visible plasmonic concepts to terahertz frequencies significantly lower than the intrinsic plasma frequency of the metal. This makes the realization of chiral SPP in the terahertz regime, similar to one on nanowire in the visible light regime, become possible. For cylindrical geometries, the geometrically induced spoof SPPs

supported by periodic groove corrugating wire have been discussed theoretically and experimentally, showing that they can enable strong confinement and focusing of the electromagnetic field [25-29]. However, the high-order SPP-like modes are of large losses [28] such that they are usually ignored and no attention is paid to chiral SPPs. Recently, a great work demonstrated that the helical groove structured metal cylinder could support chiral SPP with tuneable orbital angular momentum [30, 31], which may generate the circularly polarized terahertz wave.

2. Helically grooved metal wire waveguide for terahertz

In this paper, we provide a further discussion about the chiral SPP of a helically grooved structure on the basis of the former literature [31]. First, we present the chiral SPP, which can be excited efficiently through normally illuminating the helically grooved metal wire by using a linearly Gaussian beam. Then, the formation mechanism of groove handedness-dependent rotation of an electric field and single-stranded spiral patterns of the power flow of chiral SPP mode are discussed qualitatively and quantitatively. Finally, the evolution of the frequency-dependent circular polarization state of an electric field on the vertical cross section is analysed in detail.

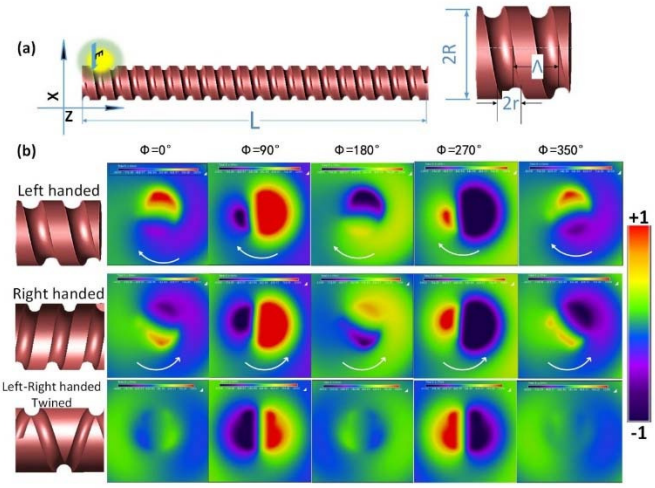

Fig. 1 Sketch of helically grooved wire and the electric patterns on the output plane at various phases for different types of helically grooved wire. (a) Helically grooved wire with geometrical parameters: radius of cylinder R, radius of the circular section of helix r, helix pitch Λ. The P-polarized (polarized perpendicularly to the Z-axis) Gaussian beam, with a waist equal to R at single frequency f_0, is normally incident at one end of the structure. (b) Real part of the longitudinal component of the electric field (Ez) versus the initial phase within a period at the output plane (10 μm away from the output end) for different structures. The upper to lower rows correspond to structures corrugated by left-handed, right-handed, and left-right twined helices, whose sketches are displayed in front of each row. The white arrows in the panels show the rotation direction of the electric field. Note that the colour scale used is adapted to the respective field intensities. Colour scale of the field intensity is from negative minimum (blue) to positive maximum (red). The values of the geometrical parameters for all cases are R=60 μm, r=25 μm, Λ=100 μm , and f_0=1 THz.

The basic model considered is a terahertz metallic wire waveguide, as shown in Fig. 1(a). Different from the traditional bare metal wire waveguide that supports a weak confined Sommerfeld wave [32] and the periodically corrugated metal wire [25, 26], the proposed wire was corrugated by a helical groove. The structure is modelled by removing a helix with a circular cross section from a cylinder. The geometry parameter is the radius of the cylinder R, total length L, radius of helix cross section r, groove period or helix pitch Λ.

To excite the surface wave, a linearly polarized Gaussian beam with a waist radius equal to the radius of the wire R is normally incident (along the X-axis direction) on one end of the helically structured wire. The chosen wave is a sinusoidal wave with a frequency f_0=1 THz. Simulations were implemented by using the FDTD program in which a three-dimensional Cartesian X-Y-Z coordinate system was used, and the axis of the wire is along the Z direction. The dimensions of the grid cells are set to 5 μm. Metal material is assumed as PEC, and the surrounding boundaries are set to be perfectly matched layers (PML). The outside dielectric is free air with a permittivity of 1. Three types of structured wire, i.e., corrugated by a single right-handed helix, single left-handed helix, and left-right-twined helix, were studied to investigate the relation between the chirality of SPP and the geometry characteristic.

3. Electric field rotation around the wire surface

Fig. 1(b) presents the evolution of the real part of the Ez field along the phase on the XY-plane placed 10 μm away from the output end for different structures at P-polarized exciting. It is found that the Ez electric field rotates along the phase for both single helix corrugated structures, shown as the first two rows in Fig. 1(b). Moreover, the rotating direction depends on the characteristic of the helical groove, i.e., the Ez field rotates clockwise for right-handed helically grooved wire and anti-clockwise for the left-handed one (all pictures are viewed in the propagation direction). Interestingly, the left-right-handed twined helically grooved wire behaves distinctively for the rotation-like behaviour disappears under the same configuration; instead, the field distribution performs like a

dipole mode. Obviously, different to real chiral SPP modes on nanowire, whose behaviours mainly depend on the incident polarization orientation [21, 22], the characteristic of chiral SPP supported by helically corrugated wire is not only related to the exciting manner but also to the handedness of the helical groove. This implies that the asymmetrical helical groove does have great influence on the SPP shape.

The formation mechanism of the rotation can be explained by the characteristic of EM fields bound to the helical structure. All of the field components in a helical geometry can be expanded in terms of the Eigenmodes as in [33]:

$$F_n(r,\phi,z) = A_n(r,z)e^{i(\pm\tilde{n}\phi+\beta z-\omega t)} \quad (1)$$

$$\tilde{n} = n + \beta\frac{\Lambda}{2\pi} \quad (2)$$

where $A_n(r,z)$ is the modal amplitude, $\tilde{n}$ is the effective mode index, which controls the symmetry properties of the EM fields, n is the integer denoting the mode order, β is the wave vector of the propagating wave, and Λ is the period of the helical geometry. Equation (1) states that components of the electromagnetic field are of azimuthal dependence with the $\tilde{n}^{th}$ modes, which are controlled by the factor $e^{i(\pm\tilde{n}\phi)}$. Effective mode index $\tilde{n}$ is a function of wave number β, implying that the number of azimuthal nodes will evolve from an even value at a small wave number to an odd value as the wave vector increases close to the band edge, $\beta = \pi/p$. This is different from the case of a bare metal cylinder, whose EM field always appears as even nodes on its azimuthal distribution [22]. For the small wave vector, the SPP mode for $n = 0$ is independent of angular, a type of quasi-symmetrical mode, which we call TM mode (note that we just call it 'TM' by borrowing the concept of modes existing on metal wire waveguides with uniform cross sections. Strictly speaking, it is not the rigorous TM mode). For $n \neq 0$, the field is in angular-dependent high mode, i.e., HE mode (we call it HE modes in the same way), which rotates clockwise or counter-clockwise at fixed cross sections where the rotation direction depends on the sign (+ or -).

In our case, the Ez field distribution on output planes for left(right)-handed cases is similar to a rotating dipole with a couple of nodes, corresponding to the HE+1(HE-1) mode or, in the strict sense, at least containing the HE mode. The disappearance of rotation for the left-right-twined grooved structure, shown in the last row, can be well understood by realizing that HE+1 and HE-1 modes, with contrary angular momentum corresponding to different handed helices, are excited out simultaneously and beat each other, resulting in the vanishing of rotation.

Actually, except for the HE mode, an azimuth-independent mode, i.e., TM mode, also exists mixed into the HE modes for the rotating field. Phase plays a fundamental role in the realization of the special mode. Generally, in HE-like mode, the transversal electric component (Ex, Ey for our case) has the same sign of the field at two sides of the cylinder, which is called phase matching (P), and the longitudinal component (Ez for our case) has the opposite sign of the field, called anti-phase matching (AP). In contrast, the TM mode behaves vice versa, i.e., the transversal field performs like AP and longitudinal field behaves like P [34]. To demonstrate phase information, the nonzero scalar components Ex, Ey and Ez on the YZ plane are shown in Fig. 2. From the pictures of the left-handed or right-handed structure, we can see that except for Ex, both the transversal component Ey and longitudinal component Ez are like neither P nor AP but like quasi-anti-phase matching (QAP), which has a small phase shift relative to P but no more than AP. This is actually the evidence of superposition of TM and HE mode, which plays a crucial role in the realization of chiral SPP mode. However, for the left-right-handed twined helically grooved structure, the appearance of P distribution for both transversal components and AP distribution for the longitudinal component (illustrated in the right column in Fig. 2) prove that it is a dipole-like mode (or non-rotating HE1 mode), considering Ez behaving as a dipole mode in the XY cross section shown in Fig. 1.

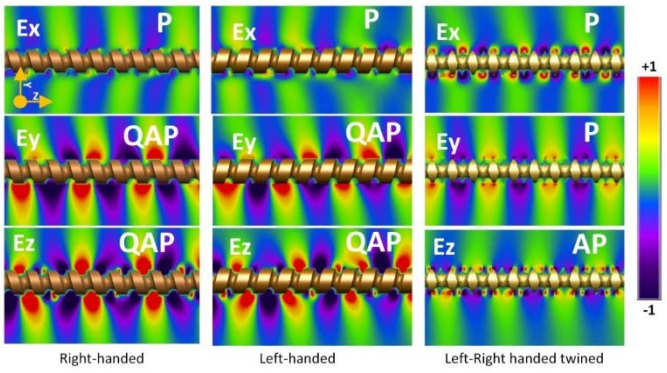

Fig. 2 Distribution of various components of electric field at initial phase on YZ cross section through the axis of three types of helically grooved wire. The symbols P, AP and QAP indicate that the E field on both sides looks like phase-matching, anti-phase matching and quasi-anti-phase matching, respectively.

4. Dispersion of SPP modes on helically grooved wire

To gain further insight into the nature of such chirality, we calculated the dispersion curves in the first Brillouin zone for a right-handed helically grooved wire wave guide using

Eigenmode solver (using the COMSOL RF module). Within all calculations, the impedance boundary condition is used to simplify the calculation, and the Drude mode of copper [35] is taken to characterize the material of the structure to consider the real metal loss. From Fig. 3, we can see that TM mode has no minimal cut-off frequency, which is in contrast to higher modes, i.e., HE mode having a minimal cut-off frequency. Moreover, the degeneracy between HE-1 mode and TM mode emerges at the band edges as a consequence of the structural chirality of the grooved wire. Insets in the figure are the mode shapes of TM (left-upper picture) and HE+1 (right-lower picture) modes at $k_z = 0.96\pi/\Lambda$, where we can see that the number of the azimuthal nodes (double the mode index) becomes odd, which is consistent with the theory that the effective mode index $\tilde{n} \approx n + 1/2$ when the wave number is close to the band edge.

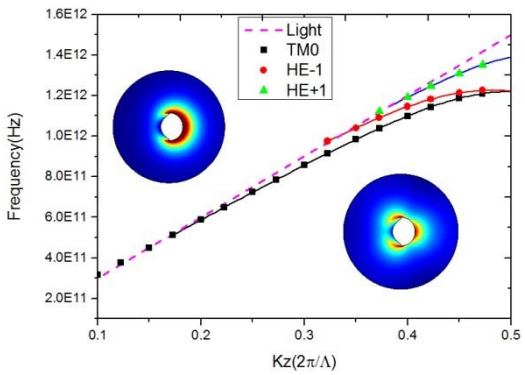

Fig. 3 Dispersion relation curve of the SPP modes supported by a right-handed helically grooved wire: cylinder with radius R=60 μm inscribed with a circular cross-section right-handed helical groove of r=25 μm, pitch Λ=100 μm. The insets display mode shapes for TM (left upper) and HE+1 (right lower) modes at $k_z = 0.96\pi/\Lambda$. Solid lines are the fitting curves.

5. Spiral power flow and frequency-dependent circular polarization on cross sections

In the case of the right-handed helically grooved wire, the incident frequency (f_0=1 THz) is above the minimal cut-off frequency of the HE-1 mode; hence, the lapped modes, evidenced by the above QAP-like phase pattern, will be generated. The electric field of the HE-1 mode having transversal rotation implies that the combination of TM and HE-1 will create a spiral distribution of electromagnetic energy density in three-dimensional space. The handedness of the spiral is also determined by the rotation direction of the included HE-1 modes. The spiral pitch can be obtained from the following expression:

$$P = 2\pi/(\beta_1 - \beta_2) \quad (3)$$

where β is the wave number of different Eigenmodes. Snapshots of Z-direction time-averaged power flow in the XZ plane for a longer right-handed case (L=10 mm, calculated using Remcom XFDTD) are presented in Fig. 4. It is obvious that a right-handed single-stranded spiral pattern is formed around the structured wire. By plotting the power energy distribution along the line at X=R+10 μm, denoted by a white dashed line, we can measure the spiral pitch, which is approximately 4.1 mm long and agrees with the calculated one derived from $P = 2\pi/(\beta_1 - \beta_2)$=4.3 mm, where the wave vector β is obtained by interpolating the dispersion curve in Fig. 3. The small departure results from the deviation of pitch measurement and wave vector interpolation.

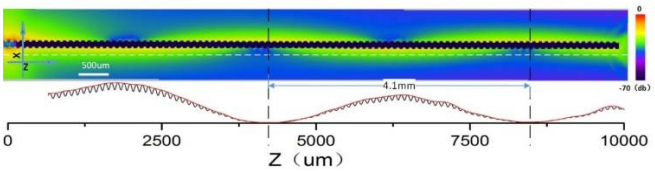

Fig. 4 Z-directional time-averaged power flow on the XY plane at 1 THz for the right-handed helically grooved wire. Lower panel is the plots (solid line is the upper enveloping line) of power varying along the line indicated by the horizontal white dashed line located at y=R+10 μm away from the wire outline. The head portion of the curve is truncated for clarity, which corresponds to the giant oscillation caused by input excitation. The measured pitch wave is approximately 4.1 mm (indicated by the vertical dashed lines). Scale bar is 500 μm. The total length of the wire is 10 mm, and other geometry parameters are identical to the above case.

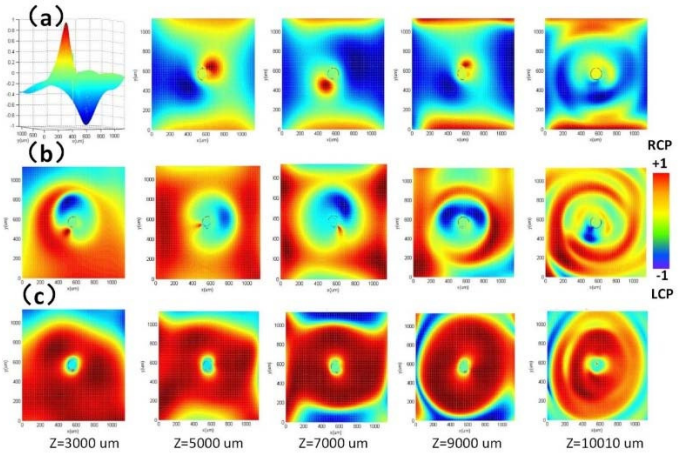

Fig. 5 Maps of degree of circular polarization C in the vertical plane at different Z locations of the right-handed helically grooved wire for different input frequencies f_0. (a) f_0= 1 THz. The polarization state rotates as the wave propagates forward.

(b) f_0 = 1.2 THz. The polarization gets complex. (c) f_0 = 1.3 THz. All of the electric field in panels (c) is perfectly right-circularly polarized around the wire. The black circles on the panels indicate the cross section of the structure. The red colour (+1) and blue colour (-1) correspond to right-circular polarization and left-circular polarization, respectively. The first picture in panel (a) is shown in 3D view to demonstrate that the peak value is almost unit. The panels listed in each column are at the same Z-location, indicated at the bottom.

In addition to the spiral power flow, chiral SPPs can also directly bring a non-linear polarization of the electric field around the outer surface. Circular polarization degree C is defined as in [36]:

$$C = \frac{2\langle E_x(t)E_y(t)\sin(\delta_x-\delta_y)\rangle}{\langle E_x^2(t)\rangle+\langle E_y^2(t)\rangle+\langle E_z^2(t)\rangle} \quad (4)$$

where $E_x(E_y), E_z$ are the transverse and longitudinal electric field components, respectively, $\langle\ \rangle$ denotes time average, and δ is the phase of the different electric field components. We calculated the degree of circular polarization degree C on different vertical cross sections for three cases of working frequency f_0=1 THz, 1.2 THz, 1.3 THz. Fig. 5 shows the spatial map of C in vertical planes of Z=3000 μm, 5000 μm, 9000 μm, and 10010 μm. Note that the vertical planes of Z =10010 μm show the map of degree of circular polarization on the outside facet, which is 10 μm away from the end of a wire whose total length is 10000 μm, as shown in Fig. 4. From the maps listed in panel (a), we can see that two peaks exist with opposite signs that correspond to left-circular and right-circular polarization, respectively. Despite the presence of a nonzero Ez component, a high degree of circular polarization is obtained ($C \approx \pm 1$ at two peaks). Interestingly, the two opposite polarization peaks also rotate along the Z axis in the same direction with the HE-1 mode, which is to say that the spatial polarization status on the vertical planes will also propagate spirally around the wire. It is worth mentioning that the polarization status will become disordered beyond the output end, shown as the rightmost picture, which is mainly because of the complex scattering at the irregular distal end. Fig. 3 reveals that the HE+1 mode is not separated from the HE-1 mode without any intersectional frequency, which implies that when the incident frequency becomes higher than the minimal cut-off frequency of the HE+1 mode and lower than the band-edge frequency of the HE-1 mode, the final electromagnetic field will be hybridized with three modes (i.e., TM, HE-1, and HE+1). To illustrate the dependence of polarization on frequency, we also mapped the polarization degree on the same planes for f_0=1.2 THz, which is located in the range occupying the three modes, shown in Fig. 5(b). It is clear that the circular polarization distribution becomes chaotic due to the more complicated EM field caused by beating of the inverse-direction rotational modes. Similarly, if the incident frequency further increases over the band-edge frequency of HE-1, the EM field will only exist in a single mode, i.e., HE+1 mode. Fig. 5(c) is the distribution of circular polarization degree for 1.3 THz that only works for the HE+1 mode. It is clear that after getting rid of the disturbing of the 'hostile' mode, a perfectly right-circular polarization was obtained around the wire due to the clockwise rotational properties of the HE+1 mode; moreover, the pure polarization state can maintain itself well along the longitudinal direction even after radiating off the output end.

6. Discussion and conclusions

The ability of converting linear polarization of the incident to circular polarization through chiral SPP makes the helically grooved wire promising for numerous applications, such as near-field optical microscopy [37] and sensors for chiral molecules [38, 39]. Moreover, the fact that the effective plasma frequency of a structured surface can be altered by redesigning the geometry of the macro-structure suggests that the chiral SPPs supported by the helically grooved wire could be adjusted. In the above discussion, we ignore the ohm loss in metal. However, related losses for a realistic metal in the terahertz region under a confined EM field become considerable. Therefore, the propagation length of chiral SPP should be considered for actual application, which can be optimized by a proper design of the geometric parameters. Actually, the polarization angle of the incident linearly polarized beam also has a great effect on chirality by determining the ratios of different component modes. Here, we only discuss one case that is perpendicular to the axis. Further discussion is underway.

In conclusion, we investigated the formation of chiral SPP on a helically corrugated wire, which is generated by normally impinging on the wire end by using a linearly polarized Gaussian wave. Different structures were compared, highlighting the crucial role of the chirality of a helical groove in the creation of rotational SPP. Both dispersion curves of such surface waves and the spiral distribution of power flow caused by chiral SPP were plotted through different numerical methods. It is shown that the spiral pitch derived from the result of the FDTD method agrees well with the one obtained from the FEM method. Moreover, highly circular polarization generated from the chiral SPP was discussed in detail, and we found that the polarization status is frequency dependent. This type of

helically grooved wire can find potential application in terahertz sensors and near-field microscopy, offering a simple way to achieve a terahertz circularly polarized light source.

Acknowledgements

We gratefully acknowledge support from the Fujian Provincial Excellent Young Scientist Fund (2014J07007), the Chancellor's Fellowship of the University of Strathclyde, the National Natural Science Foundation of China (51005077), the Training Program of Fujian Excellent Talents in Universities, the Specialised Research Fund for the Doctoral Program of Higher Education, the Ministry of Education, P. R. China (20133514110008), and the Ministry of Health, P. R. China (WKJ-FJ-27).

References

1.Shen, Y., et al., Detection and identification of explosives using terahertz pulsed spectroscopic imaging. Applied Physics Letters, 2005. 86(24): p. 241116.

2.Leahy Hoppa, M., et al., Wideband terahertz spectroscopy of explosives. Chemical Physics Letters, 2007. 434(4): p. 227-230.

3.Kawase, M., et al., Non-Destructive Evaluation Method of Pharmaceutical Tablet by Terahertz-Time-Domain Spectroscopy: Application to Sound-Alike Medicines. Journal of Infrared Millimeter and Terahertz Waves, 2013. 34(9): p. 566-571.

4.Zhong, S., et al., Non-destructive quantification of pharmaceutical tablet coatings using terahertz pulsed imaging and optical coherence tomography. Optics and Lasers in Engineering, 2011. 49(3): p. 361-365.

5.Falconer, R.J. and A.G. Markelz, Terahertz spectroscopic analysis of peptides and proteins. Journal of Infrared, Millimeter, and Terahertz Waves, 2012. 33(10): p. 973-988.

6.Nagel, M., et al., A functionalized THz sensor for marker-free DNA analysis. Physics in Medicine and Biology, 2003. 48(22): p. 3625.

7.Walther, M., et al., Collective vibrational modes in biological molecules investigated by terahertz time - domain spectroscopy. Biopolymers, 2002. 67(4 - 5): p. 310-313.

8.Ferguson, B. and X.-C. Zhang, Materials for terahertz science and technology. Nature materials, 2002. 1(1): p. 26-33.

9.Siegel, P.H. Terahertz technology in biology and medicine. in Microwave Symposium Digest, 2004 IEEE MTT-S International. 2004. IEEE.

10.Tang, Y. and A.E. Cohen, Enhanced Enantioselectivity in Excitation of Chiral Molecules by Superchiral Light. Science, 2011. 332(6027): p. 333-336.

11.Hendry, E., et al., Ultrasensitive detection and characterization of biomolecules using superchiral fields. Nature Nanotechnology, 2010. 5(11): p. 783-787.

12.Tang, Y. and A.E. Cohen, Optical Chirality and Its Interaction with Matter. Physical Review Letters, 2010. 104(16).

13.Gansel, J.K., et al., Gold Helix Photonic Metamaterial as Broadband Circular Polarizer. Science, 2009. 325(5947): p. 1513-1515.

14.Fan, Z. and A.O. Govorov, Plasmonic Circular Dichroism of Chiral Metal Nanoparticle Assemblies. Nano Letters, 2010. 10(7): p. 2580-2587.

15.Gramotnev, D.K. and S.I. Bozhevolnyi, Plasmonics beyond the diffraction limit. Nature Photonics, 2010. 4(2): p. 83-91.

16.Barnes, W.L., A. Dereux, and T.W. Ebbesen, Surface plasmon subwavelength optics. Nature, 2003. 424(6950): p. 824-830.

17.Shegai, T., et al., Unidirectional Broadband Light Emission from Supported Plasmonic Nanowires. Nano Letters, 2011. 11(2): p. 706-711.

18.Li, Z., et al., Effect of a proximal substrate on plasmon propagation in silver nanowires. Phys Rev B, 2010. 82(24): p. 241402.

19.Lal, S., S. Link, and N.J. Halas, Nano-optics from sensing to waveguiding. Nature photonics, 2007. 1(11): p. 641-648.

20.Schmidt, M.A. and P.S.J. Russell, Long-range spiralling surface plasmon modes on metallic nanowires. Optics Express, 2008. 16(18): p. 13617-13623.

21.Zhang, S., et al., Chiral surface plasmon polaritons on metallic nanowires. Physical review letters, 2011. 107(9): p. 096801.

22.Chen, C.-M., et al., Spiral surface plasmon modes on uniform and tapered metallic nanorods. JOSA B, 2013. 30(9): p. 2529-2534.

23.Pendry, J., L. Martin-Moreno, and F. Garcia-Vidal, Mimicking surface plasmons with structured surfaces. Science, 2004. 305(5685): p. 847-848.

24.Maier, S.A., Plasmonics: Fundamentals and Applications: Fundamentals and Applications. 2007: Springer.

25.Maier, S.A., et al., Terahertz surface plasmon-polariton propagation and focusing on periodically corrugated metal wires. Physical Review Letters, 2006. 97(17): p. 176805.

26.Fernández-Domínguez, A., et al., Spoof surface plasmon polariton modes propagating along periodically corrugated wires. Selected Topics in Quantum Electronics, IEEE Journal of, 2008. 14(6): p. 1515-1521.

27.Jiang, T., et al., High-order modes of spoof surface plasmon polaritons on periodically corrugated metal surfaces. Progress In Electromagnetics Research M, 2009. 8: p. 91-102.

28.Shen, L., et al., Effect of absorption on terahertz surface plasmon polaritons propagating along periodically corrugated metal wires. Physical Review B, 2008. 77(7): p. 075408.

29.Ganti, S., et al., Characterization and Modeling of Laser Micromachined Periodically Corrugated Metallic Terahertz Wire

Waveguides. Journal of Infrared, Millimeter, and Terahertz Waves, 2012. 33(11): p. 1104-1116.

30.Fernández-Domínguez, A., et al., Terahertz surface plasmon polaritons on a helically grooved wire. Applied Physics Letters, 2008. 93(14): p. 141109.

31.Rüting, F., et al., Subwavelength chiral surface plasmons that carry tuneable orbital angular momentum. Physical Review B, 2012. 86(7): p. 075437.

32.Jeon, T.-I., J. Zhang, and D. Grischkowsky, THz Sommerfeld wave propagation on a single metal wire. Applied Physics Letters, 2005. 86(16): p. 161904-161904-3.

33.Crepeau, P. and P.R. McIsaac, Consequences of symmetry in periodic structures. Proceedings of the IEEE, 1964. 52(1): p. 33-43.

34.Zaccaria, R.P., et al., Surface plasmon polariton compression through radially and linearly polarized source. Optics letters, 2012. 37(4): p. 545-547.

35.Ordal, M., et al., Optical properties of the metals al, co, cu, au, fe, pb, ni, pd, pt, ag, ti, and w in the infrared and far infrared. Applied Optics, 1983. 22(7): p. 1099-1119.

36.Biagioni, P., et al., Cross Resonant Optical Antenna. Physical Review Letters, 2009. 102(25).

37.Schnell, M., et al., Nanofocusing of mid-infrared energy with tapered transmission lines. Nature photonics, 2011. 5(5): p. 283-287.

38.Tang, Y. and A.E. Cohen, Optical chirality and its interaction with matter. Physical review letters, 2010. 104(16): p. 163901.

39.Xu, J., et al. Terahertz circular dichroism spectroscopy of biomolecules. in Optical Technologies for Industrial, Environmental, and Biological Sensing. 2004. International Society for Optics and Photonics.